# Enhancing Phase Separation and Photovoltaic Performance of All-Conjugated Donor−Acceptor Block Copolymers with Semifluorinated Alkyl Side Chains

Florian Lombeck,[†,‡] Hartmut Komber,[§] Alessandro Sepe,[||] Richard H. Friend,[†] and Michael Sommer*[,‡,⊥,#]

[†]Optoelectronics Group, Cavendish Laboratory, University of Cambridge, J. J. Thomson Avenue, Cambridge CB3 0HE, U.K.

[‡]Makromolekulare Chemie, Universität Freiburg, Stefan-Meier-Straße 31, 79104 Freiburg, Germany

[§]Leibniz-Institut für Polymerforschung Dresden e.V., Hohe Straße 6, 01069 Dresden, Germany

[||]Adolphe Merkle Institute, Chemin des Verdiers 4, CH-1700, Fribourg, Switzerland

[⊥]Freiburger Materialforschungszentrum, Stefan-Meier-Straße 21, 79104 Freiburg, Germany

[#]FIT, Freiburger Zentrum für interaktive Werkstoffe und bioinspirierte Technologien, Georges-Köhler-Allee 105, 79110 Freiburg, Germany

**S** *Supporting Information*

**ABSTRACT:** Phase separation of all-conjugated donor−acceptor block copolymers is more difficult to achieve compared to classical coil−coil systems owing the intrinsic similarity of the two blocks having both rigid conjugated backbones and alkyl side chains and their generally low degrees of polymerization. Here we demonstrate that side chain fluorination of a poly(carbazole-*alt*-dithienylbenzothiadiazole) segment (SF-PCDTBT), to be used as electron acceptor block in combination with poly(3-hexylthiophene) P3HT as donor block in all-conjugated donor−acceptor block copolymers of type SF-PCDTBT-*b*-P3HT, strongly increases



Increasing crystallinity, phase separation, PCE

dissimilarity between P3HT and SF-PCDTBT leading to phase separation for already moderate molar masses. Key to the successful synthesis of a new TBT-monomer with semifluorinated side chains is a direct arylation step that elegantly bypasses classical cross-coupling reactions in which the semifluorinated side chain causes low yields. Suzuki polycondensation of the semifluorinated TBT monomer with a suitable carbazole comonomer and in situ termination by P3HT-Br is optimized extensively with respect to the yield of the end-capping efficiency and molar mass control of the PCDTBT segment. When the fluorinated side chains are replaced by hydrogen (H-PCDTBT) or by *n*-hexyl chains (hex-PCDTBT), the tendency for phase separation with covalently connected P3HT is much reduced as shown by differential scanning calorimetry and grazing incidence small-angle scattering measurements on thin films. Favorably, of all the block copolymers made only SF-PCDTBT-*b*-P3HT is microphase separated, exhibits face-on orientation of P3HT domains, and additionally displays surface segregation of the SF-PCDTBT segment at the polymer/air interface. All of these properties are beneficial for single layer single component solar cells. SF-PCDTBT-*b*-P3HT exhibits the best solar cells performance with a high open-circuit voltage of 1.1 V and a power conversion efficiency of ∼1% which largely outperforms devices based on the analogous H-PCDTBT-*b*-P3HT and hex-PCDTBT-*b*-P3HT.
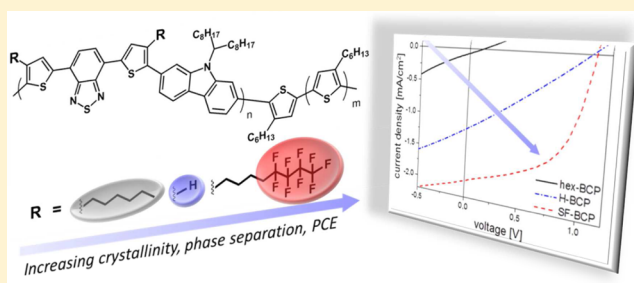
## INTRODUCTION

Conjugated polymers have attracted considerable attention within the last two decades due to their feasible integration into lightweight, flexible, and transparent electronic devices such as organic field-effect transistors (OFETs), organic light-emitting diodes (OLEDs), and organic photovoltaic cells (OPVs), owing to their good charge carrier mobilities, bright and tunable light emission, and broad absorption in the visible range of the electromagnetic spectrum.[1−5] A major advantage compared to inorganic semiconductors is the processability of organic semiconductors from solution enabling lower manufacturing costs and high throughput device fabrication via multiple printing techniques. To date, various p-type polymers are known while the majority of high performance OPV devices utilize soluble fullerene derivatives as n-type material in the active layer.[6] A notable and—for light harvesting devices—important drawback of fullerenes is the weak light absorption in the visible and near IR regions. An alternative that bypasses the poor contribution of fullerenes to the photocurrent is the implementation of n-type polymers. Potential advantages

**Scheme 1. Synthesis Routes to the Semifluoroalkylated Monomer SF-TBT (10)**[a]
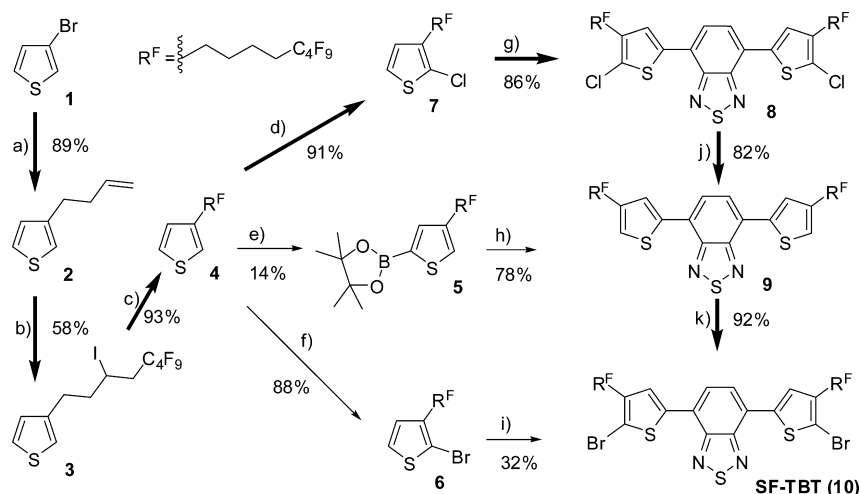


[a]Reagents and conditions: (a) But-3-enylmagnesium bromide, 1 mol % Ni(dppp)Cl$_2$, THF, room temperature, 24 h, 89%; (b) I—C$_4$F$_9$, 15 mol % AIBN, 3 d, 70 °C, 68%; (c) NaBH$_4$, DMSO, 4 h, 80 °C, 93%; (d) NCS, CHCl$_3$/acetic acid, 50 °C, 20 h, 91%; (e) LiTMP, THF, −78 °C, 5 h, $^i$PrOBpin, room temperature, 10 h, 14%; (f) NBS, THF, room temperature, 20 h, 88%; (g) Br$_2$BT, PivOH, K$_2$CO$_3$, Pd(OAc)$_2$, PCy$_3$, DMAc, 75°C, 3 d, 86%; (h) Br$_2$BT, Pd$_2$(dba)$_3$, SPhos, Aliquat 336, tol/2 M K$_2$CO$_3$, 80 °C, 3 h, $\mu$W, 78%; (i) Br$_2$BT, PivOH, K$_2$CO$_3$, Pd(OAc)$_2$, PCy$_3$, DMAc, 65°C, 6d, 32%; (j) KO$^t$Bu, $^i$PrOH, PEPPSI-$^i$Pr, 30 h, room temperature, 82%; (k) NBS, THF, room temperature, 20 h, 92%.
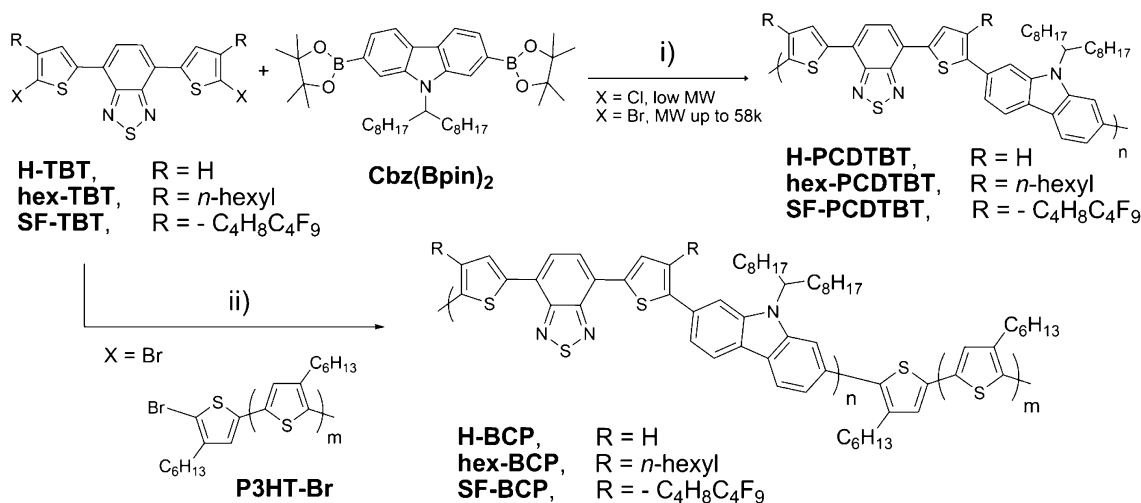
offered by this approach are a more efficient, ideally complementary light absorption of both components and a relatively high open-circuit voltage which is not limited by the energy levels of fullerenes. Yet more important to efficient operation of polymer solar cells is a nanoscale active layer morphology with stable and bicontinuous transport pathways for both electrons and holes. The morphology of all-polymer blends relies on their demixing behavior during spin-casting, whereby the common strategy is the empirical correlation of kinetically trapped structures with performance.[7−11] In polymer−polymer blends, empirically optimized morphologies are realized through processing and postprocessing treatments such as casting solvent,[12,13] additives,[8,14,15] thermal annealing,[16] and solvent vapor swelling.[17]

Block copolymers (BCPs) self-assemble into well-ordered and thermodynamically stable nanostructures with domain sizes commensurate to the exciton diffusion length,[18,19] and hence have been considered ideal for OPV applications.[20−24] Nevertheless, due to synthetic challenges only a limited number of fully conjugated donor−acceptor BCPs have been reported.[25−34] To achieve efficient charge separation, reduce recombination and enable charge transport, bicontinuous interpenetrating donor−acceptor networks having sharp interfaces are key for photovoltaic applications. However, for all-conjugated block copolymers where both donor and acceptor blocks are conjugated and in many cases equipped with hydrocarbon side chains, sufficient dissimilarity between the two segments might not readily be given. In such a case, microphase separation can be induced driven by crystallization or additionally by side chain engineering to increase the Flory−Huggins interaction parameter.[25,28] While in all-polythiophene block copolymers different side chains have been shown to lead to phase separation, this approach is much less explored for donor−acceptor all-conjugated block copolymers.[35] Alternatively, one segment can be changed from a main-chain block to side-chain pendants, however in this instance transport might be intrinsically limited by hopping events between pendants.[36]

An efficient approach to increase incompatibility of block copolymer segments is the introduction of fluorinated units. Indeed, nonconjugated block copolymers show drastically increased $\chi$ values with increasing fluorination.[37] Along the same lines, polythiophenes with alternating alkyl and semi-fluoroalkyl side chains form structures with alternating alkyl and semifluoroalkyl layers.[38] These results suggest that side chain fluorination of one of the segments in all-conjugated donor−acceptor block copolymers is a promising strategy to realize microphase separated nanostructures for already low degrees of polymerization usually present in conjugated polymers. Here, we report the synthesis, characterization and photovoltaic performance of the first all-conjugated donor−acceptor block copolymers having a semifluorinated (SF) PCDTBT-based acceptor block and a P3HT donor block. Compared to the alkylated and nonsubstituted PCDTBT analogues, P3HT is able to crystallize quantitatively in SF-PCDTBT-b-P3HT, a result which is perfectly in line with the highest photovoltaic performance among the three, thus confirming our approach of using fluorinated alkyl chains in all-conjugated donor−acceptor block copolymers to increase dissimilarity of the two conjugated blocks and finally to enable thermodynamically stable bicontinuous morphologies suitable for both charge separation and charge transport.

## ■ RESULTS AND DISCUSSION

PCDTBT is commonly used as p-type material in combination with fullerenes; however, when combined with P3HT, it acts as acceptor forming a type II heterojunction.[39] The LUMO−LUMO and HOMO−HOMO level offsets are 0.9 and 0.6 eV, respectively, providing sufficient driving force for charge separation.[9,40] In addition, PCDTBT exhibits excellent chemical and photostability.[41] Recently, we found that all-conjugated block copolymers of type F8TBT-b-P3HT did not microphase separate for the molecular weights and compositions investigated, and we rationalized that the similarity in chemical structure between the two segments was the underlying reason.[28] On the basis of these results, we

**Scheme 2. Copolymer and Block Copolymer Synthesis**[a]



H-TBT, R = H
hex-TBT, R = *n*-hexyl
SF-TBT, R = - C$_4$H$_8$C$_4$F$_9$

Cbz(Bpin)$_2$

X = Cl, low MW
X = Br, MW up to 58k

H-PCDTBT, R = H
hex-PCDTBT, R = *n*-hexyl
SF-PCDTBT, R = - C$_4$H$_8$C$_4$F$_9$

X = Br

P3HT-Br

H-BCP, R = H
hex-BCP, R = *n*-hexyl
SF-BCP, R = - C$_4$H$_8$C$_4$F$_9$

[a]Reaction conditions: (i) 8 equiv of Cs$_2$CO$_3$, Pd(PPh$_3$)$_4$, THF, 80 °C, 3 d; (ii) 4−17.5 mol % P3HT-Br, 8 equiv of Cs$_2$CO$_3$, Pd(PPh$_3$)$_4$, THF, 80 °C, 3 d.

redesigned an all-conjugated block copolymer structure by (i) replacing the hexyl side chains of the thiophene rings in F8TBT by semifluorinated alkyl side chains and by (ii) replacing the fluorene unit by carbazole. The latter substitution was chosen on the basis that blends of P3HT and PCDTBT showed slightly enhanced performance compared to F8TBT/P3HT.[8] While P3HT is no longer the most efficient donor material for OPV, its unsurpassed virtue lies in its easy availability, molar mass control and end group functionalization.[42−46] In our study, the TBT unit of the PCDTBT block is equipped with either *n*-hexyl (hex-PCDTBT) or semifluorinated (SF-PCDTBT) side chains or is unsubstituted (H-PCDTBT). Generally, the substituent on the TBT unit greatly enhance solubility and thus facilitates analysis, however as mentioned the incorporation of hexyl side chains leads to greater similarity with P3HT. Thus, semifluorinated alkyl side chains on the TBT unit increase both solubility as well as dissimilarity with P3HT. To maintain electronic structure of PCDTBT, an alkyl chain segment must be introduced between the backbone and the perfluorinated alkyl segment, leading to a semifluorinated alkyl side chain structure. Initially synthesized TBT monomers with ethylene alkyl spacer-based semifluorinated side chains were unstable. Thus, a butylene spacer was placed between the thiophene ring and the perfluorobutyl segment resulting in the new monomer structure SF-TBT (**10**) (Scheme 1).

**Monomer Synthesis.** The semifluoroalkylated thiophene building block **4** was synthesized starting from 3-bromothiophene (**1**) in three steps in 56% overall yield according to Collard et al.[47] (Scheme 1). Subsequent borylation of **4** to form **5** turned out to be a great challenge. First, **4** is less reactive than nonfluorinated analogue 3-alkylthiophenes (3AT). Reaction conditions converting 3AT to the monoborylated product in 90% yield[48] gave 16% yield of **5** only. Second, bulky bases, such as lithiumdiisopropylamid (LDA) or lithium tetramethylpiperidide (LiTMP), also significantly deprotonate the sterically more hindered 2-position of the thiophene ring resulting in regioisomers. Third and most importantly, the gamma-protons of the perfluorinated side chain exhibit substantial acidity. Hence, the elimination of the perfluorocarbon segment and recovery of **2** was found to be a considerable side reaction. Increasing the reaction temperature enhances the reaction rate,

but favors elimination over borylation. Alternative borylation reactions, such as iridium-catalyzed direct C−H-activated borylation following literature procedures did not furnish **5**.[49] A solution to this issue was found in the direct C−H-arylation (DA) reaction of monochlorinated thiophene **7** thus elegantly bypassing the borylation step. **7** was prepared from **4** by chlorination with NCS in 91% yield. The chlorine substituent blocks the 2-position but itself is not reactive under appropriate direct arylation conditions at moderate temperature, thus avoiding oligomerization and the formation of regioisomers.[50] Additionally, the 2-chloro substituent activates the 5-position of **7** for DA compared to **4**.[51] DA reaction of **7** with 4,7-dibromo-2,1,3-benzothiadiazole (Br$_2$BT) resulted in the dichlorinated compound **8** in 86% yield.[50] **8** can directly be used as monomer, however Suzuki polycondensation conditions of **8** with 9-(heptadecan-9-yl)-2,7-bis(4,4,5,5-tetramethyl-1,3,2-dioxaborolan-2-yl)-9H-carbazole (Cbz(Bpin)$_2$) could be optimized to moderate molar masses of $M_n$ = 10 kg/mol only. Hence, **8** was dechlorinated catalytically with a *N*-heterocyclic carbene-palladium complex, PEPPSI-$^i$Pr, as catalyst, potassium *tert*-butanolate as base and 2-propanol as reducing agent to give **9** in 82% yield.[52] Upon dibromination with NBS the final monomer SF-TBT (**10**) formed in 92% yield. A shortcut to SF-TBT is the bromination of **4** followed by a DA. **4** was brominated with NBS in THF to give **6** in 88% yield. The DA of **6** with Br$_2$BT was done under the same conditions but at lower temperature than **7**. However, the yield of SF-TBT obtained by this route was 32% only due to the possibility of oligo- and polymerization of **6** arising from the higher reactivity of the C−Br bond in **6** compared to the C−Cl bond in **7**.[53]

**(Block) Copolymer Synthesis.** Suzuki polycondensation (SPC) is a simple, versatile and straightforward method to synthesize conjugated donor−acceptor copolymers from two symmetric monomers with complementary functionalities, i.e. an aryl dibromide and an aryl with two boronic acid or ester groups. Monomer purity, a precise 1:1-stoichiometry of the monomers and minimized side reactions are required to obtain defect-free, high molecular weight (MW) polymer samples.[54,55] A recently published protocol to prepare PCDTBT and its hexyl-analogue, hereinafter referred to as hex-PCDTBT, with high MW from the dichlorinated TBT monomer could not

### Table 1. Reaction Conditions Used for BCP Syntheses[a]

| entry | BCP-type | catalyst (Pd:L 1:2) | mol % P3HT-Br[b] | base/solvent | Đ[c] | $M_n$[c] (kg/mol) | wt % P3HT[d] |
|---|---|---|---|---|---|---|---|
| 1 | hex-BCP | $Pd_2(dba)_3$/$PPh_3$ | 5 | $K_2CO_3$/tol | 1.51 | 18.0 | – |
| 2 | hex- BCP | $Pd_2(dba)_3$/XPHOS | 5 | $K_2CO_3$/tol | 1.64 | 16.4 | – |
| 3 | hex-BCP | $Pd_2(dba)_3$/SPHOS | 5 | $K_2CO_3$/tol | 1.72 | 22.6 | – |
| 4 | hex-BCP | $Pd_2(dba)_3$/brettPHOS | 5 | $K_2CO_3$/ tol | 1.60 | 19.3 | – |
| 5 | hex-BCP | $Pd_2(dba)_3$/$PCy_3$ | 5 | $K_2CO_3$/ tol | 1.44 | 11.2 | – |
| 6 | hex-BCP | $Pd(dppf)Cl_2$ | 5 | $K_2CO_3$/ tol | 2.29 | 32.6 | – |
| 7 | hex-BCP | $Pd(PPh_3)_4$ | 5 | $K_2CO_3$/ tol | 1.75 | 26.4 | 20 |
| 8 | hex-BCP | $Pd(PPh_3)_4$ | 7.5 | $K_2CO_3$/ tol | 2.51 | 22.2 | 32 |
| 9 | hex-BCP | $Pd(PPh_3)_4$ | 10 | $K_2CO_3$/ tol | 1.85 | 21.7 | 39 |
| 10 | hex-BCP | $Pd(PPh_3)_4$ | 12.5 | $K_2CO_3$/ tol | 1.87 | 19.4 | 46 |
| 11 | hex-BCP | $Pd(PPh_3)_4$ | 15 | $K_2CO_3$/ tol | 1.97 | 18.9 | 56 |
| 12 | hex-BCP | $Pd(PPh_3)_4$ | 17.5 | $K_2CO_3$/ tol | 1.94 | 17.3 | 72 |
| 13 | hex-BCP | $Pd(PPh_3)_4$ | 7.5 | CsF/THF | 1.80 | 29.8 | – |
| 14 | hex-BCP | $Pd(PPh_3)_4$ | 7.5 | $Cs_2CO_3$/THF | 2.08 | 32.5 | 42 |
| 15 | hex-BCP | $Pd(PPh_3)_4$ | 8 | $Cs_2CO_3$/THF | 2.11 | 21.6 | 48 |
| 16 | H-BCP | $Pd(PPh_3)_4$ | 5 | $K_2CO_3$/tol | 1.72 | 23.8 | 36 |
| 17 | SF-BCP | $Pd(PPh_3)_4$ | 8 | CsF/THF | 1.54 | 26.0 | 46 |
| 18 | SF-BCP | $Pd(PPh_3)_4$ | 7.5 | $Cs_2CO_3$/THF | 1.68 | 26.6 | 43 |
| 19 | SF-BCP | $Pd(PPh_3)_4$ | 5 | CsF/THF | 1.68 | 29.2 | 29 |
| 20 | SF-BCP | $Pd(PPh_3)_4$ | 6.5 | $Cs_2CO_3$/THF | 2.17 | 29.3 | 43 |
| 21 | SF-BCP | $Pd(PPh_3)_4$ | 5 | $Cs_2CO_3$/THF | 1.82 | 32.9 | 38 |
| 22 | SF-BCP | $Pd(PPh_3)_4$ | 4 | $Cs_2CO_3$/THF | 1.76 | 35.8 | 34 |

[a]In all cases a P3HT-Br macroinitiator with $M_n$ 14.0 kg/mol, Đ 1.07 was used. [b]In mol % with respect to 100% $Cbz(Bpin)_2$. [c]Values calculated from SEC detected at 254 nm. [d]Values calculated from ^{1}H NMR backbone signal intensities.

successfully be applied to SF-TBT **8** as only oligomers were obtained.[45] Solvent variations and mixtures with fluorinated aromatic solvents, such as trifluorobenzene or 1,4-bis-(trifluoromethyl)benzene, did not lead to number-average molecular weights $M_n > 10$ kg/mol. Applying SPC standard procedures[50,55,56] to make PCDTBT-based structures with the semifuoroalkylated and dibrominated monomer SF-TBT resulted in copolymers with enhanced but still moderate $M_n$ < 15 kg/mol. The usage of a 1:1-mixture of toluene and 1,4-bis(trifluoromethyl)benzene as solvent, 2 M $K_2CO_3$ aqueous base and $Pd(PPh_3)_4$ as catalyst increased the MW to $M_n$= 28 kg/mol, and changing the biphasic system to pure THF in combination with CsF further raised $M_n$ to 31 kg/mol with a dispersity Đ = 1.95. Upon exchanging the base to $Cs_2CO_3$, SF-PCDTBT with a satisfying $M_n$ = 38 kg/mol and Đ = 1.52 was obtained. SF-PCDTBT exhibits excellent solubility in chloroform or THF at room temperature (Scheme 2, reaction i.

In order to couple monobrominated P3HT-Br to SF-PCDTBT, two methods were tested in which P3HT-Br was either added in the beginning or at late stage of the Suzuki polycondensation.[26,28] The latter method was unsuccessful and led to a high content of unreacted P3HT-Br and debrominated P3HT-H. To avoid extensive optimization including the identification of end groups with time, we followed the second approach, in which P3HT-Br was added as end-capper to the initial equimolar mixture of SF-TBT and $Cbz(Bpin)_2$ already in the beginning (Scheme 2, reaction (ii). In this instance, it is possible to tune the size of the SF-PCDTBT block by varying the initial amount of P3HT-Br as stoichiometry is disturbed, whereby an increasing amount of P3HT-Br lowers the PCDTBT block length and vice versa.[27] The additional bromine functionality induces an overall stoichiometric mismatch resulting in reduced MWs of the acceptor-block,[54] while P3HT segment length can be adjusted easily beforehand.[42]

To find the most efficient conditions for P3HT end-capping, different phosphine ligands and palladium precursors were tested for BCP synthesis using hex-PCDTBT as model system (see Table 1, entries 1−7). The resulting BCPs are referred to as hex-BCPs. The SEC traces of the resulting products are compared to the P3HT-Br and shown in Figure SI-4 (Supporting Information). All polymerizations with aromatic phosphines resulted in monomodal SEC traces, while the use of aliphatic tricyclohexylphosphine ($PCy_3$) in combination with tris(dibenzylideneacetone)dipalladium ($Pd_2(dba)_3$) gave bimodal distributions with low MWs. The highest MWs were obtained using [1,1′-bis(diphenylphosphino)ferrocene]-dichloro-palladium ($Pd(dppf)Cl_2$) as catalyst, followed by tetrakis(triphenylphosphine)palladium ($Pd(PPh_3)_4$) and the Buchwald ligands SPHOS, XPHOS and brettPHOS[57] in combination with $Pd_2(dba)_3$ as palladium source. $Pd(PPh_3)_4$ gives higher MWs than $PPh_3$ in combination with $Pd_2(dba)_3$, 46.8 kg/mol and 27.1 kg/mol respectively, indicating insufficient *in situ* formation of the active catalyst species from the $Pd_2(dba)_3$ precursor.[58] This is in line with Schlüter who mentioned that $Pd(PPh_3)_4$ needs to be prepared freshly to obtain efficient catalysts.[54] All BCP samples exhibit excellent solubility in THF or chloroform. Using the unsubstituted TBT monomer in combination with the optimized conditions for block copolymer formation results in an H-BCP which is poorly soluble in chloroform, but processable from 1,2-dichlorobenzene (Table 1, entry 16).

The success of the BCP synthesis was analyzed by size exclusion chromatography (SEC) measurements with detection at three distinctive wavelengths. The detection wavelengths were chosen at 254 nm, where the absorption of both polymers is almost equal, at 418 nm, where PCDTBT has a local absorption minimum while the P3HT absorption is close to its absorption maximum, and at 580 nm, where P3HT does not absorb light (Supporting Information, Figure SI-4). Thus, a
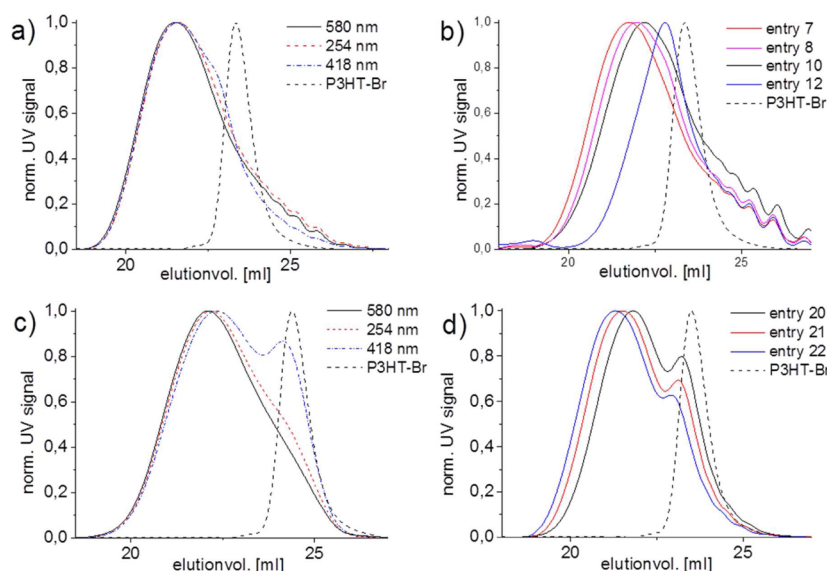
**Figure 1.** (a) SEC traces of a hex-BCP (entry 8) detected at 254 nm, 418 and 580 nm and of the P3HT-Br macroinitiator; (b) elugrams of hex-BCPs with different acceptor block lengths detected at 254 nm; (c) SEC traces of SF-BCP (entry 17) detected at 254, 418, and 580 nm; (d) elugrams of SF-BCPs with different acceptor block lengths detected at 418 nm.

substantial overlap of the eluograms detected at these three wavelengths indicate minimal P3HT homopolymer contaminants. Figure 1a shows the results of the reaction with Pd(PPh$_3$)$_4$ as catalyst (entry 8), indicating successful BCP formation with negligible side reactions. However, eluogram intensity at volumes greater than P3HT-Br indicated some minor PCDTBT homopolymer. Importantly, all other combinations of catalyst precursor and ligand resulted in polymer mixtures whose SEC traces at 418 nm exhibit low-MW shoulders indicating P3HT homopolymer residues, which was confirmed by NMR spectroscopy. The synthetic approach could in principle lead to additional triblock copolymer formation, which is challenging to quantify. We assume that the formation of triblock structures of type P3HT-*b*-PCDTBT-*b*-P3HT is unlikely due to the small molar stoichiometric excess of bromide functions used (see Table 1).

After identification of Pd(PPh$_3$)$_4$ as the most efficient catalyst, control over MW of the hex-PCDTBT segment was elucidated (see Table 1, entries 7−12; Figure 1b). The mole (weight) fraction of added P3HT-Br was varied from 5% (20%) to 17.5% (70%). Upon decreasing the amount of P3HT-Br the overall molecular weight increased (Figure 1b). The same trend and the ability to adjust the acceptor block size can be seen for SF-PCDTBT-*b*-P3HT. However, for the fluorinated BCP mixtures a shoulder at lower MWs in the SEC traces, detected at 418 nm, indicated a small content of P3HT homopolymer (Figure 1c,d). $^1$H NMR end group analysis revealed debromination as the origin for the observed nonreacted P3HT homopolymer. Deconvolution of the constituent peaks in the SEC trace reveals <20 wt % P3HT homopolymer impurities with respect to the total amount of P3HT.

The successful formation of block copolymers could also be proved by $^1$H NMR spectroscopy (Figure 2). Figure 2a depicts the enlarged region of the P3HT-Br backbone signal with characteristic signals of the bromine and hydrogen terminated chains.[28] Upon copolymerization with SF-TBT and Cbz-(Bpin)$_2$, the signals related to Br-termination disappear and a similar signal pattern appears in the 7.12−7.18 ppm region (Figure 2b). Such a shift of this signal pattern was also observed
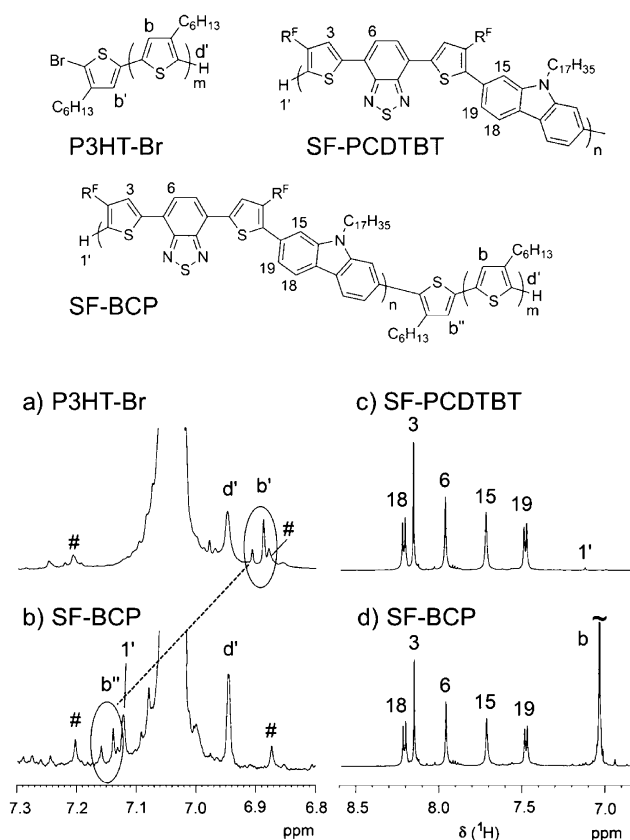


**Figure 2.** $^1$H NMR spectra (regions) and chemical structures of (a) P3HT-Br macroinitiator (entry 26) showing the signals of H- (d′) and Br-termination (b′, circled). b) Signal shift due to formation of the P3HT-Cbz block junction (b″, circled). The regions of aromatic protons of SF-PCDTBT (entry 25) and SF-BCP (entry 20) are depicted in parts c and d, respectively. # marks $^{13}$C satellite signals. Solvent: C$_2$D$_2$Cl$_4$ at 120 °C.

for structural similar PF8TBT-*b*-P3HT diblock copolymers[28] and is characteristic for uniform substitution of bromine by the
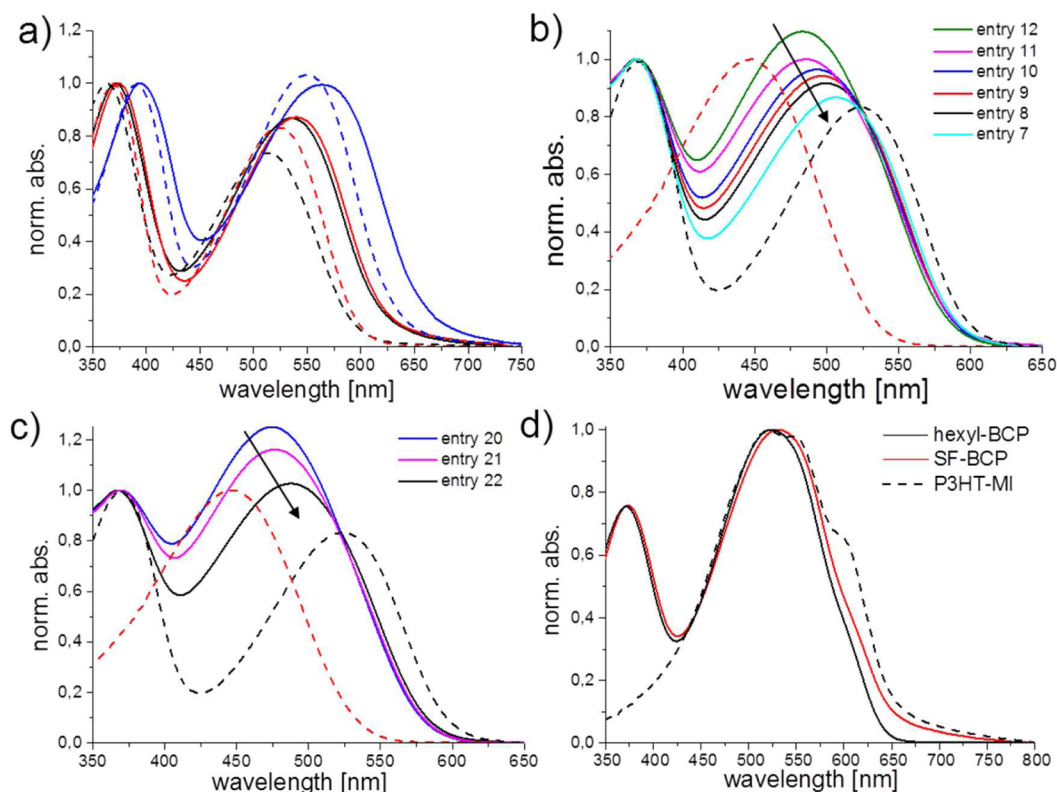
**Figure 3.** (a) Steady-state UV−vis absorption spectra of H-PCDTBT (blue), hex-PCDTBT (red), and SF-PCDTBT (black) in the solid state (solid) and chlorobenzene solution (dashed); (b) UV−vis absorption spectra of hex-BCPs with different acceptor block lengths (entries 7−12, solid), hex-PCDTBT (dashed, black), and P3HT (dashed, red) in chloroform solution, the arrow displays increasing hex-PCDTBT block length; (c) UV−vis absorption spectra of SF-BCPs with different acceptor block lengths (entries 20−22, solid), SF-PCDTBT (dashed, black) and P3HT (dashed, red) in chlorobenzene solution, the arrow displays increasing SF-PCDTBT block length; (d) UV−vis absorption spectra of a hex-BCP and SF-BCP with comparable donor−acceptor weight composition (entries 10 and 17, solid) and the P3HT-Br macroinitiator (dashed).
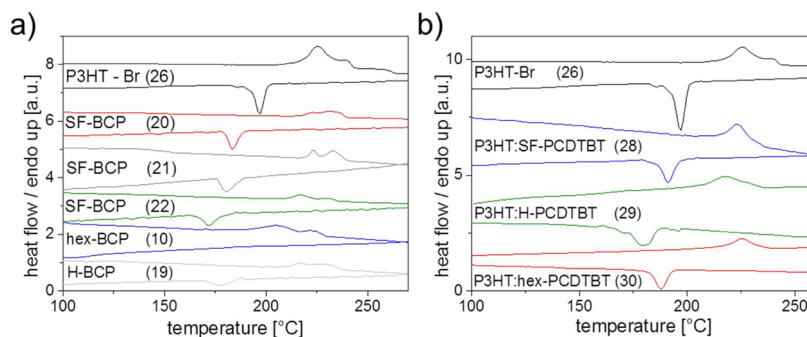


**Figure 4.** DSC curves of (a) P3HT-Br macroinitiator (entry 26), SF-BCP (entries 20−22), hex-BCP (entry 10), H-BCP (entry 16) and (b) P3HT-Br macroinitiator (entry 26) and the corresponding blends SF-PCDTBT:P3HT (entry 27), H-PCDTBT:P3HT (entry 28), and hex-PCDTBT:P3HT (entry 29) scanned at 10 K/min.

first Cbz unit of the SF-PCDTBT block and thus represents the Cbz-P3HT block junction. The signal at 7.12 ppm results from H-TBT termination of the SF-PCDTBT block. Finally, Figure 2d depicts all aromatic protons signals of SF-PCDTBT-*b*-P3HT (entry 20). Besides the backbone signals of the SF-PCDTBT block (cf. Figure 2c, entry 25), the signal of the P3HT backbone appears at 7.05 ppm. The copolymer composition was determined from $^1$H NMR signal integrals of both blocks.

**Optical and Thermal Properties of PCDTBT-*b*-P3HT.** UV−vis absorption spectra of the block copolymers and of the individual homopolymers are investigated and compared qualitatively (Figure 3). The spectra of hex-PCDTBT (Figure 3a, red) and SF-PCDTBT (Figure 3a, black) are almost

identical, confirming that the butyl spacer electronically insulates the backbone from the perfluorinated segment. Owing to better planarization due to less steric hindrance caused by solubilizing side chains, the charge-transfer (CT) band of unsubstituted H-PCDTBT is stronger and red-shifted (Figure 3a, blue).[59] P3HT exhibits a broad absorption peak at 445 nm while hex- and SF-PCDTBT exhibit two absorption peaks at 369 nm ($\pi-\pi^*$ transition) and 523 nm (CT band) in solution (Figure 3b,c, dashed lines). Both hex-BCP (Figure 3b) and SF-BCP (Figure 3c) materials are superpositions of the contributions from P3HT and PCDTBT according to their weight fractions. In Figure 3d, representative solid state absorption profiles of hex-BCP and SF-BCP with comparable

**Table 2. Overview of Physical and Thermal Block Copolymer Characterization**[a]

| entry | type | $M_n$[b] (GPC, 254 nm) | Đ | wt % P3HT | $T_m$ [°C] | $T_c$ [°C] | $\Delta H_m$ [J/g] | $\Delta H_c$ [J/g] | % abs cryst[c] |
|---|---|---|---|---|---|---|---|---|---|
| 7 | hex-BCP | 26.4 | 1.75 | 20 | 205.3 | – | 1.6 | – | 24 |
| 8 | hex-BCP | 22.2 | 2.51 | 32 | 200.8 | – | 2.7 | – | 25 |
| 9 | hex-BCP | 21.7 | 1.85 | 39 | 204.1 | – | 3.3 | – | 25 |
| 10 | hex-BCP | 19.4 | 1.87 | 46 | 206.8 | – | 4.2 | – | 27 |
| 11 | hex-BCP | 18.9 | 1.97 | 56 | 209.9 | – | 6.3 | – | 34 |
| 12 | hex-BCP | 17.3 | 1.94 | 72 | 210.3 | 125.7 | 8.6 | 1.9 | 36 |
| 16 | H-BCP | 20.8 | 1.72 | 36 | 218.1 | 182.4 | 7.3 | 7.5 | 43 |
| 17 | SF-BCP | 26.0 | 1.54 | 46 | 231.6 | 183.5 | 9.5 | 9.8 | 62 |
| 18 | SF-BCP | 26.6 | 1.68 | 43 | 217.3 | 171.7 | 8.3 | 8.6 | 57 |
| 19 | SF-BCP | 29.2 | 1.68 | 29 | 233.0 | 180.3 | 5.0 | 4.9 | 52 |
| 20 | SF-BCP | 29.3 | 2.17 | 43 | 213.9 | 179.3 | 8.8 | 8.1 | 62 |
| 21 | SF-BCP | 32.9 | 1.82 | 38 | 223.8 | 182.8 | 7.3 | 7.1 | 59 |
| 22 | SF-BCP | 35.8 | 1.76 | 34 | 231.4 | 184.8 | 6.4 | 6.0 | 57 |
| 23 | hex-PCDTBT | 46.9 | 2.14 | 0 | – | – | – | – | – |
| 24 | H-PCDTBT | 26.8 | 3.22 | 0 | – | – | – | – | – |
| 25 | SF-PCDTBT | 37.1 | 1.59 | 0 | – | – | – | – | – |
| 26 | P3HT-Br MI | 14.1 | 1.07 | 100 | 225.3 | 196.6 | 21.0 | 18.0 | 64 |
| 27 | blend P3HT:SF-PCDTBT | 30.3 | 1.93 | 50 | 224.1 | 190.9 | 10.4 | 9.9 | 64 |
| 28 | blend P3HT:H-PCDTBT | 21.1 | 2.20 | 50 | 216.5 | 179.4 | 9.7 | 8.2 | 59 |
| 29 | blend P3HT:hex-PCDTBT | 45.8 | 1.89 | 50 | 225.2 | 187.8 | 9.4 | 6.0 | 58 |

[a]All BCPs were synthesized using P3HT-Br with $M_{n,NMR}$= 14 kg/mol; the same P3HT-Br was used in the physical blends. [b]Values given in kg/mol. [c]Using $\Delta H_m$ and 33 J/g for a 100% crystalline P3HT sample.[61]

donor−acceptor ratios (Table 1, entries 10 and 17) and the pristine P3HT block are shown. The peak of the BCP is red-shifted upon fluorination, from 526 to 531 nm, and the contribution of the P3HT shoulder at lower energies is more distinct in the SF-BCP indicating increased P3HT crystallinity in the fluorinated BCPs compared to the nonfluorinated analogues.

To further elucidate the phase separation behavior induced by the SF-PCDTBT segment and to confirm the enhanced P3HT crystallinity in SF-BCP materials, differential scanning calorimetry (DSC) was carried out (Figure 4). Both hex- and SF-PCDTBT copolymers did not show detectable thermal transitions and are amorphous. The used macroinitiator P3HT-Br exhibits melting and crystallization temperatures $T_m$ and $T_c$ at 225 and 197 °C, respectively, and melting and crystallization enthalpies $\Delta H_m$ and $\Delta H_c$ of 21.0 J/g and 18.0 J/g, respectively (Figure 4a). $\Delta H_m$ values for a 100% crystalline P3HT sample have been extrapolated to 37 J/g and 33 J/g based on solid-state NMR and WAXS measurements, respectively.[60,61] Using 33 J/g obtained from temperature-dependent WAXS measurements,[61] absolute degrees of crystallinity for all materials containing P3HT are given in Table 2. All SF-PCDTBT-b-P3HT samples exhibited melting temperatures between 220 and 230 °C and thus values very similar compared to the transition of P3HT. Interestingly, the P3HT block in SF-BCPs recrystallized when cooling at 10 K/min with a $\Delta H_c$ between 4.9 J/g and 9.8 J/g for SF-BCPs containing 29% and 46% P3HT, respectively. These values could be indicative for a microphase separated melt from which crystallization can readily occur. The $\Delta H_c$ values indicate that 52−62% of P3HT in the BCP are crystalline. Considering that the used P3HT-Br end-capper has a degree of crystallinity of 64%, we conclude that almost the same amount of P3HT chains can crystallize in the block copolymer compared to P3HT end-capper. All SF-BCPs feature a crystallization temperature below 190 °C indicating that the covalent linking slows down crystallization. The values for $\Delta H_c$ of P3HT in the SF-PCDTBT-b-P3HT

block copolymers correlate nicely with the weight fraction of P3HT. The melting temperature $T_m$ increases upon increasing SF-PCDTBT block length (see Table 2, entry 20−22 and Supporting Information, Figure SI-3). In stark contrast, all hex-BCPs showed strongly decreased melting points between 200 and 210 °C. P3HT crystallization was not observed in the hex-BCP analogues under the same conditions, indicating that this process was possibly hindered due to the presence of a homogeneous melt. Such a behavior was already observed for PF8TBT-b-P3HT and is caused by the presence of the 3-hexylthiophene motif both in hex-PCDTBT and P3HT, leading to reduced dissimilarity and a smaller interaction parameter.[28] The nonfluorinated hex-BCP samples exhibit much lower degrees of crystallinity between 24−36%, and the H-BCP exhibited 43% (entries 7−12 and 16). The thermal transitions of the BCPs were compared to physical 1:1 blends of P3HT and SF-, hex- and H-PCDTBT, respectively. In the SF-PCDTBT blend, the values for $T_m$ and $\Delta H_m$ of P3HT (224 °C and 10.4 J/g) are almost the same compared to pristine P3HT-Br (225 °C and 21.0 J/g) (Figure 4a), suggesting that the crystallizable amount of P3HT is the same in the P3HT-Br end-capper and in the blend. These values were slightly reduced in blends with hex-PCDTBT and H-PCDTBT (9.4 J/g and 9.7 J/g, respectively, Table 2).

Taken together, from the thermal data, it can be concluded that the presence of semifluorinated alkyl side chains in contrast to hexyl side chains greatly enhances incompatibility of the donor and acceptor segments, which leads to much improved crystallinities of the P3HT block and concomitant to that, to better phase separation and purer domains.

**Morphological and Photovoltaic Properties of PCDTBT-b-P3HT.** To investigate the microphase behavior of the novel PCDTBT-b-P3HT materials, AFM was carried out (Figure 5). It can be seen that, after film annealing at 250 °C with the temperature being chosen based on thermal transitions of the BCP, no well-defined surface morphology can be found in all samples. For hex-BCP, the surface morphology is flat and
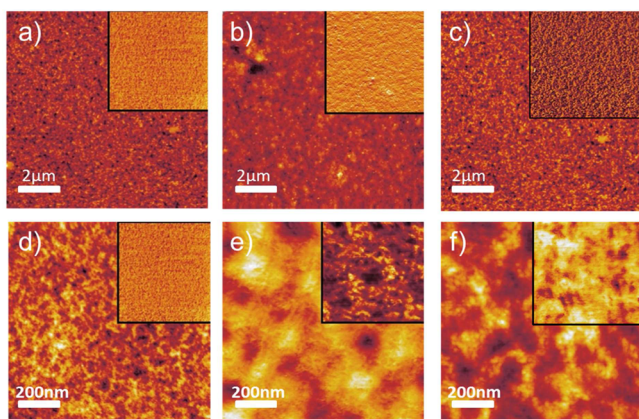
**Figure 5.** AFM height images (inset phase image) of hex-BCP (a, d; entry 9), H-BCP (b, e; entry 16) and SF-BCP (c, f; entry 22); the AFM image dimensions are 10 $\mu$m × 10 $\mu$m (top: a, b, c) and 1 $\mu$m × 1 $\mu$m (bottom: d, e, f).

featureless (Figure 5a,c), and on the basis of DSC results, it can be assumed that the BCP segments are well intermixed. The surface morphology shows significant coarsening in the case of H-BCP (Figure 5b,d) and more pronounced for SF-BCP (Figure 5c,f). Contact angle measurements indicate a capping layer of the SF-PCDTBT segment. The contact angles of a water droplet on P3HT, SF-PCDTBT and SF-PCDTBT-b-P3HT were found to be 106°, 121°, and 120°, respectively. Hence, the hydrophobicity of the BCP film surface is comparable to the neat SF-PCDTBT film surface and preferential arrangement of the semifluorinated block at the film−air interface can be deduced. However, given the thermal data of the BCP materials, it can be assumed that these are microphase separated and that imaging by surface sensitive techniques such as AFM does not reveal this information owing to the presence of a SF-PCDTBT capping layer. This situation is ideal for photovoltaics, where on the one hand pure domains are needed to avoid charge trapping and recombination, while on the other hand surface segregation of the acceptor block is beneficial in standard device architectures to avoid surface recombination.

To obtain more detailed structural insights, on both morphology and crystallinity of the thin films, films of hex-BCP (entry 9), H-BCP (entry 16), and SF-BCP (entry 22) were additionally studied by grazing incidence small- and wide-angle X-ray scattering (GISAXS and GIWAXS, respectively). The GISAXS and GIWAXS spectra shown in Figure 6 exhibit

prominent Bragg reflections at positions which correspond to *d*-spacing and lattice structure of the corresponding thin films, thus employing a wide *q*-range where structural properties are completely investigated. Hex-BCP and H-BCP show a similar scattering pattern in the GISAXS profile where no indication for a phase separated structure was found (Figure 6a). Hex-BCP and H-BCP showed GIWAXS spectra revealing edge-on orientation of P3HT crystals with a main chain-side chain separation (100 peak) of 1.7 nm (Figure 6b and c). On the other hand, the GISAXS pattern of SF-BCP exhibited a broad signal indicating microphase separation on a length scale of 9.5 nm (Figure 6a, red). While this GISAXS feature is very broad and the length scale of 9.5 nm is clearly too short for what could be expected on the basis of a fully extended chain, these measurements clearly show marked differences of SF-BCP compared to the nonfluorinated BCPs. Further studies devoted to effects of block copolymer dispersity and rigid linker will shine light on this behavior and are ongoing. Additionally and in strong contrast to the nonfluorinated BCPs, P3HT crystals are now face-on oriented (Figure 6, parts b and c).

Finally, OPV devices were fabricated from all BCP samples using the standard device architecture glass/ITO/PE-DOT:PSS/BCP/Al. Representative *J*−*V* curves are shown in Figure 7a and device characteristics are summarized in Table 3. To investigate the effect of the enhanced phase separation behavior of the SF-BCP materials induced by semifluoroalkyl side chains, all active layers were postannealed for 20 min at 250 °C, i.e., above the melting temperature $T_m$ of the P3HT segment, and slowly cooled to room temperature. All hex-BCPs exhibited extremely poor device characteristics with power conversion efficiencies (PCEs) below 0.003% with an external quantum efficiency (EQE) below 1% as a result of substantial intermixing of hex-PCDTBT and P3HT block segments at the molecular scale. The H-BCP with the unsubstituted H-PCDTBT segment showed a PCE of 0.37% after postannealing. However, both these performances were clearly outperformed by the SF-BCP (entry 22) for which average device efficiencies of 0.95% were measured (Figure 7a and Table 3). The EQE of both H-BCP and SF-BCP starts at 670 nm although the absorption of H-PCDTBT is red-shifted compared to SF-PCDTBT. While the shoulder at ~610 nm in both EQE curves indicate significant contribution of P3HT to the photocurrent, maximum EQE values of the H-BCP device did not exceed 9%. In contrast, the EQE of SF-BCP reached the best value among all block copolymers exhibiting 16.5% (Figure 7b), a result that is fully in line with the *J*−*V* characteristics and the scattering data. For a consistent comparison, however, different block
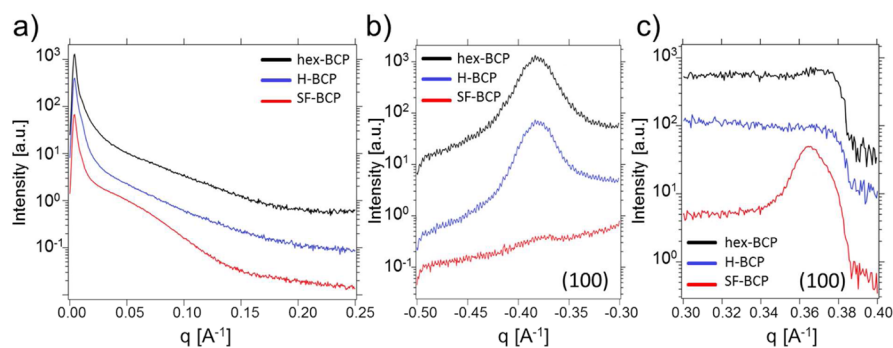


**Figure 6.** (a) 1D GISAXS intensity profiles as a function of the scattering vector *q* of the three thin films. Corresponding 1D GIWAXS profiles for (b) in-plane and (c) out-of-plane *a*-axis of hex-BCP (entry 9, black), H-BCP (entry 16, blue) and SF-BCP (entry 22, red).
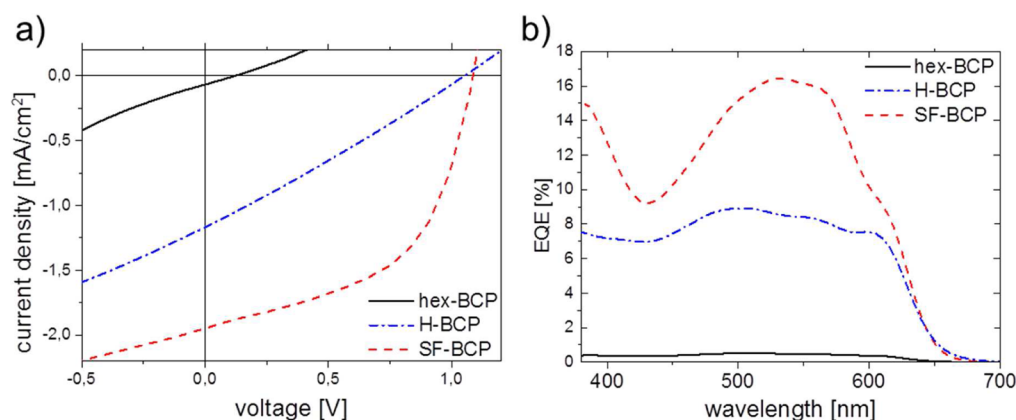
**Figure 7.** (a) Current−voltage and (b) EQE characteristics of OPV devices with hex-BCP (entry 9, black), H-BCP (entry 16, blue), and SF-BCP (entry 22, red) as active layer material.

**Table 3. Average Device Characteristics of Block Copolymer Solar Cells**

| sample | $V_{oc}$ [V] | $J_{sc}$ [mA/cm$^2$] | fill factor | PCE [%] |
|---|---|---|---|---|
| hex-BCP (entry 9) | 0.14 ± 0,03 | −0.067 ± 0,05 | 0.28 ± 0.09 | 0.0028 ± 0.002 |
| H-BCP (entry 16) | 1.12 ± 0,08 | −1.33 ± 0,3 | 0.37 ± 0.03 | 0.55 ± 0.18 |
| SF-BCP (entry 22) | 1.08 ± 0,02 | −1.95 ± 0,4 | 0.45 ± 0.05 | 0.95 ± 0.28 |

copolymer compositions and molecular weights need to be investigated in detail. Nevertheless, the DSC and GISAXS/GIWAXS results point out that SF-BCP shows a very strong tendency to phase separate resulting in a micro phase separated nanostructure with a preferential P3HT crystal orientation that is highly beneficial to OPV performance, while both H-BCP and Hex-BCP analogues suffer from reduced phase separation, a P3HT crystal orientation not favorable for OPV performance, and thus drastically lowered PCEs.

## CONCLUSION

We have presented the synthesis and detailed characterization of a series of novel all-conjugated block copolymers with a semifluoroalkylated SF-PCDTBT segment as acceptor block and P3HT as donor block, and have compared their properties and phase behavior to block copolymer analogues having either no (H-BCP) or hexyl substituents (hex-BCP) on the TBT unit in the PCDTBT segment. Crucial to the successful synthesis of the new semifluoroalkylated TBT monomer is a direct arylation step instead of traditional reactions which fail in this instance. DSC measurements indicate almost quantitative recrystallization of the P3HT block in SF-BCP. By contrast, P3HT crystallinity in hex-BCP and H-BCP is drastically lowered caused by (partial) miscibility between the two segments. GISAXS and GIWAXS measurements reveal a phase separated structure for SF-BCP with a spacing of 9.5 nm, while no such phase separation behavior was found in scattering measurements for hex-BCP and H-BCP. Furthermore, P3HT domains are face-on oriented in films of SF-BCP and edge-on oriented in H-BCP and hex-BCP. As a result of the beneficial phase behavior of SF-PCDTBT-*b*-P3HT, the performance of OPV devices is superior compared to hex-BCP and H-BCP. Additionally, SF-PCDTBT forms a capping layer in thin films of SF-PCDTBT-*b*-P3HT at the polymer air interface which is beneficial for preventing surface recombination in standard device architectures. This study highlights side chain fluorination as an efficient strategy to increase the Flory−Huggins interaction parameter between donor−acceptor all-conjugated

copolymers to achieve microphase separated structures that are purer and expected to exhibit sharp domain boundaries. This is especially important considering the generally small degrees of polymerization of conjugated polymer segments present in all-conjugated block copolymers, and their naturally similar structures arising from the general design principle of a conjugated backbone and alkyl substituents, both of which decrease the tendency for microphase separation.

## ASSOCIATED CONTENT

### Ⓢ Supporting Information

The Supporting Information is available free of charge on the ACS Publications website at DOI: 10.1021/acs.macromol.5b01845.

> Experimental section, syntheses, NMR spectra, and SEC traces (PDF)

## AUTHOR INFORMATION

### Corresponding Author

*(M.S.) michael.sommer@makro.uni-freiburg.de.

## ACKNOWLEDGMENTS

## REFERENCES

(1) Facchetti, A. *Mater. Today* **2013**, *16* (4), 123−132.

(2) Wang, C.; Dong, H.; Hu, W.; Liu, Y.; Zhu, D. *Chem. Rev.* **2012**, *112* (4), 2208−2267.

(3) Sekine, C.; Tsubata, Y.; Yamada, T.; Kitano, M. S.; Doi, S. *Sci. Technol. Adv. Mater.* **2014**, *15* (3), 034203.

(4) Zhu, X.-H.; Peng, J.; Cao, Y.; Roncali, J. *Chem. Soc. Rev.* **2011**, *40* (7), 3509−3524.

(5) Jou, J.-H.; Kumar, S.; Agrawal, A.; Li, T.-H.; Sahoo, S. *J. Mater. Chem. C* **2015**, *3*, 2974−3002.

(6) Po, R.; Bianchi, G.; Carbonera, C.; Pellegrino, A. *Macromolecules* **2015**, *48* (3), 453−461.

(7) Thompson, B. C.; Fréchet, J. M. J. *Angew. Chem., Int. Ed.* **2008**, *47* (1), 58−77.

(8) Liu, X.; Huettner, S.; Rong, Z.; Sommer, M.; Friend, R. H. *Adv. Mater.* **2012**, *24* (5), 669−674.

(9) McNeill, C. R.; Halls, J. J. M.; Wilson, R.; Whiting, G. L.; Berkebile, S.; Ramsey, M. G.; Friend, R. H.; Greenham, N. C. *Adv. Funct. Mater.* **2008**, *18* (16), 2309−2321.

(10) Zhou, E.; Cong, J.; Wei, Q.; Tajima, K.; Yang, C.; Hashimoto, K. *Angew. Chem., Int. Ed.* **2011**, *50* (12), 2799−2803.

(11) Liu, Y.; Larsen-Olsen, T. T.; Zhao, X.; Andreasen, B.; Søndergaard, R. R.; Helgesen, M.; Norrman, K.; Jørgensen, M.; Krebs, F. C.; Zhan, X. *Sol. Energy Mater. Sol. Cells* **2013**, *112*, 157−162.

(12) Chang, L.; Lademann, H. W.; Bonekamp, J. B.; Meerholz, K.; Moulé, A. J. *Adv. Funct. Mater.* **2011**, *21* (10), 1779−1787.

(13) Pavlopoulou, E.; Kim, C. S.; Lee, S. S.; Chen, Z.; Facchetti, A.; Toney, M. F.; Loo, Y. *Chem. Mater.* **2014**, *26*, 5020−5027.

(14) Lou, S. J.; Szarko, J. M.; Xu, T.; Yu, L.; Marks, T. J.; Chen, L. X. *J. Am. Chem. Soc.* **2011**, *133* (51), 20661−20663.

(15) Hu, S.; Dyck, O.; Chen, H.; Hsiao, Y.; Hu, B.; Duscher, G.; Dadmun, M.; Khomami, B. *RSC Adv.* **2014**, *4* (53), 27931.

(16) Padinger, F.; Rittberger, R. S.; Sariciftci, N. S. *Adv. Funct. Mater.* **2003**, *13* (1), 85.

(17) Sepe, A.; Rong, Z.; Sommer, M.; Vaynzof, Y.; Sheng, X.; Müller-Buschbaum, P.; Smilgies, D.-M.; Tan, Z.-K.; Yang, L.; Friend, R. H.; Steiner, U.; Huettner, S. *Energy Environ. Sci.* **2014**, *7* (5), 1725.

(18) Leibler, L. *Macromolecules* **1980**, *13* (10), 1602−1617.

(19) Bates, F. S.; Fredrickson, G. H. *Phys. Today* **1999**, *52* (2), 32−38.

(20) Segalman, R.; McCulloch, B.; Kirmayer, S.; Urban, J. J. *Macromolecules* **2009**, *42* (23), 9205−9216.

(21) Topham, P. D.; Parnell, A. J.; Hiorns, R. C. *J. Polym. Sci., Part B: Polym. Phys.* **2011**, *49* (16), 1131−1156.

(22) Sommer, M.; Huettner, S.; Thelakkat, M. *J. Mater. Chem.* **2010**, *20* (48), 10788.

(23) Sommer, M.; Huettner, S.; Thelakkat, M. *Adv. Polym. Sci.* **2010**, *228*, 123−153.

(24) Shah, M.; Ganesan, V. *Macromolecules* **2010**, *43*, 543−552.

(25) Mulherin, R. C.; Jung, S.; Huettner, S.; Johnson, K.; Kohn, P.; Sommer, M.; Allard, S.; Scherf, U.; Greenham, N. C. *Nano Lett.* **2011**, *11* (11), 4846−4851.

(26) Guo, C.; Lin, Y. H.; Witman, M. D.; Smith, K.; Wang, C.; Hexemer, A.; Strzalka, J.; Gomez, E. D.; Verduzco, R. *Nano Lett.* **2013**, *13* (6), 2957−2963.

(27) Ku, S.; Brady, M. A.; Treat, N. D.; Cochran, J. E.; Robb, M. J.; Kramer, E. J.; Chabinyc, M. L.; Hawker, C. J. *J. Am. Chem. Soc.* **2012**, *134* (28), 16040−16046.

(28) Sommer, M.; Komber, H.; Huettner, S.; Mulherin, R.; Kohn, P.; Greenham, N. C.; Huck, W. T. S. *Macromolecules* **2012**, *45* (10), 4142−4151.

(29) Scherf, U.; Gutacker, A.; Koenen, N. *Acc. Chem. Res.* **2008**, *41* (9), 1086−1097.

(30) Ahmed, E.; Morton, S. W.; Hammond, P. T.; Swager, T. M. *Adv. Mater.* **2013**, *25* (32), 4504−4510.

(31) Izuhara, D.; Swager, T. M. *Macromolecules* **2011**, *44*, 2678−2684.

(32) Tu, G.; Li, H.; Forster, M.; Heiderhoff, R.; Balk, L. J.; Scherf, U. *Macromolecules* **2006**, *39* (13), 4327−4331.

(33) Woody, K. B.; Leever, B. J.; Durstock, M. F.; Collard, D. M. *Macromolecules* **2011**, *44*, 4690−4698.

(34) Wang, J.; Ueda, M.; Higashihara, T. *ACS Macro Lett.* **2013**, *2* (6), 506−510.

(35) Lee, E.; Hammer, B.; Kim, J. K.; Page, Z.; Emrick, T.; Hayward, R. C. *J. Am. Chem. Soc.* **2011**, *133* (27), 10390−10393.

(36) Lohwasser, R. H.; Gupta, G.; Kohn, P.; Sommer, M.; Lang, A. S.; Thurn-Albrecht, T.; Thelakkat, M. *Macromolecules* **2013**, *46* (11), 4403−4410.

(37) Hillmyer, M.; Lodge, T. P. *J. Polym. Sci., Part A: Polym. Chem.* **2002**, *40* (1), 1−8.

(38) Wang, B.; Watt, S.; Hong, M.; Domercq, B.; Sun, R.; Kippelen, B.; Collard, D. M. *Macromolecules* **2008**, *41* (14), 5156−5165.

(39) Wang, Y.; Wang, Q.; Zhan, X.; Wang, F.; Safdar, M.; He, J. *Nanoscale* **2013**, *5* (18), 8326−8339.

(40) Park, S. H.; Coates, N.; Moon, J. S.; Cho, S.; Roy, A.; Beaupre, S.; Moses, D.; Leclerc, M.; Lee, K.; Heeger, A. J. *Nat. Photonics* **2009**, *3*, 297−302.

(41) Peters, C. H.; Sachs-Quintana, I. T.; Kastrop, J. P.; Beaupré, S.; Leclerc, M.; McGehee, M. D. *Adv. Energy Mater.* **2011**, *1* (4), 491−494.

(42) Kiriy, A.; Senkovskyy, V.; Sommer, M. *Macromol. Rapid Commun.* **2011**, *32*, 1503−1517.

(43) Kohn, P.; Huettner, S.; Komber, H.; Senkovskyy, V.; Tkachov, R.; Kiriy, A.; Friend, R. H.; Steiner, U.; Huck, W. T. S.; Sommer, J.; Sommer, M. *J. Am. Chem. Soc.* **2012**, *134*, 4790.

(44) Lohwasser, R. H.; Thelakkat, M. *Macromolecules* **2011**, *44* (9), 3388−3397.

(45) Miyakoshi, R.; Yokoyama, A.; Yokozawa, T. *J. Am. Chem. Soc.* **2005**, *127* (49), 17542−17547.

(46) Osaka, I.; McCullough, R. D. *Acc. Chem. Res.* **2008**, *41*, 1202−1214.

(47) Hong, X. M.; Tyson, J. C.; Collard, D. M. *Macromolecules* **2000**, *33* (10), 3502−3504.

(48) Li, J. C.; Lee, S. H.; Hahn, Y. B.; Kim, K. J.; Zong, K.; Lee, Y. S. *Synth. Met.* **2008**, *158* (3−4), 150−156.

(49) Chotana, G.; Kallepalli, V.; Maleczka, R. E.; Smith, M. R. *Tetrahedron* **2008**, *64* (26), 6103−6114.

(50) Lombeck, F.; Matsidik, R.; Komber, H.; Sommer, M. *Macromol. Rapid Commun.* **2015**, *36* (2), 231−237.

(51) Liégault, B.; Petrov, I.; Gorelsky, S. I.; Fagnou, K. *J. Org. Chem.* **2010**, *75* (4), 1047−1060.

(52) Navarro, O.; Marion, N.; Oonishi, Y.; Kelly, R. A., III; Nolan, S. P. *J. Org. Chem.* **2006**, *71*, 685−692.

(53) Rudenko, A. E.; Wiley, C. a.; Tannaci, J. F.; Thompson, B. C. *J. Polym. Sci., Part A: Polym. Chem.* **2013**, *51* (12), 2660−2668.

(54) Schlüter, A. D. *J. Polym. Sci., Part A: Polym. Chem.* **2001**, *39*, 1533−1556.

(55) Sakamoto, J.; Rehahn, M.; Wegner, G.; Schlüter, a D. *Macromol. Rapid Commun.* **2009**, *30* (9−10), 653−687.

(56) Blouin, N.; Michaud, A.; Leclerc, M. *Adv. Mater.* **2007**, *19* (17), 2295−2300.

(57) Surry, D. S.; Buchwald, S. L. *Angew. Chem., Int. Ed.* **2008**, *47* (34), 6338−6361.

(58) Amatore, C.; Jutand, A. *Coord. Chem. Rev.* **1998**, *178-180*, 511−528.

(59) Kim, J.; Kwon, Y. S.; Shin, W. S.; Moon, S.-J.; Park, T. *Macromolecules* **2011**, *44* (7), 1909−1919.

(60) Pascui, O. F.; Lohwasser, R. H.; Sommer, M.; Thelakkat, M.; Thurn-Albrecht; Saalwächter, K. *Macromolecules* **2010**, *43*, 9401−9410.

(61) Balko, J.; Lohwasser, R. H.; Sommer, M.; Thelakkat, M.; Thurn-Albrecht, T. *Macromolecules* **2013**, *46* (24), 9642−9651.